THE JOURNAL OF PHYSICAL CHEMISTRY B

Article

pubs.acs.org/JPCB

Describing Two-Photon Absorptivity of Fluorescent Proteins with a New Vibronic Coupling Mechanism

M. Drobizhev,*[,†] N. S. Makarov,[‡] S. E. Tillo,[§] T. E. Hughes,[∥] and A. Rebane[†,⊥]

[†]Department of Physics, Montana State University, Bozeman, Montana, USA

[‡]School of Chemistry and Biochemistry, Georgia Institute of Technology, Atlanta, Georgia, USA

[§]Vollum Institute, Oregon Health and Science University, Portland, Oregon, USA

[∥]Department of Cell Biology and Neuroscience, Montana State University, Bozeman, Montana, USA

[⊥]National Institute of Chemical Physics and Biophysics, Tallinn, Estonia

Supporting Information

ABSTRACT: Fluorescent proteins (FPs) are widely used in two-photon microscopy as genetically encoded probes. Understanding the physical basics of their two-photon absorption (2PA) properties is therefore crucial for creation of two-photon brighter mutants. On the other hand, it can give us better insight into molecular interactions of the FP chromophore with a complex protein environment. It is known that, compared to the one-photon absorption spectrum, where the pure electronic transition is the strongest, the 2PA spectrum of a number of FPs is dominated by a vibronic transition. The physical mechanism of such intensity redistribution is not understood. Here, we present a new physical model that explains this effect through the "Herzberg–Teller"-type vibronic coupling of the difference between the permanent dipole moments in the ground and excited states ($\Delta\boldsymbol{\mu}$) to the bond-length-alternating coordinate. This model also enables us to quantitatively describe a large variability of the 2PA peak intensity in a series of red FPs with the same chromophore through the interference between the "Herzberg–Teller" and Franck–Condon terms.

$$\sigma_2 = A\left[\underbrace{\Delta\mu_e^{\,2}(Q_a^0)K(\nu)}_{Franck-Condon} + \underbrace{\left(\frac{\partial(\Delta\mu_e)}{\partial Q_a}\right)^2 \frac{\hbar}{4\pi M_a \nu_a} K(\nu-\nu_a)}_{"Herzberg-Teller"}\right]$$

1. INTRODUCTION

Two-photon absorption (2PA) spectra of a number of fluorescent proteins (FPs),[1−9] synthetic analogues of their chromophores,[10] as well as common ionic (and zwitterionic) fluorescent dyes[11−21] show an intriguing feature: their longest-wavelength 2PA maximum is always shifted to the blue with respect to twice the corresponding one-photon absorption (1PA) peak wavelength; see Figure 1 for an example. This effect is found in the spectra of fluorescent proteins with different chromophores but only when the chromophore is in its anionic state[9] or, more specifically, capable of charge-transfer (CT) resonance (Figure 1, upper panel). It is due to a dominance of a vibronic, 0−1, transition in the 2PA spectrum as compared to the 1PA spectrum where the pure electronic, 0−0, transition dominates.[1,6] Despite the generality of this effect, its physical mechanism is not fully understood. Another rather unexpected finding is that the intensity of the vibronically induced 2PA peak strongly varies in the series of red fluorescence proteins,[9] including DsRed2,[22] mRFP,[23] and Fruits mutants,[24] all containing the same chromophore structure shown in Figure 1, which we call red FP chromophore in what follows.

The goal of this work is to present an explicit physical model that can (1) explain the dominance of the vibronic 0−1 transition in the 2PA spectrum of a chromophore with CT resonance, (2) quantitatively describe the dependence of its intensity on local electric field, and (3) eventually be used to make predictions about how to further intensify the peak 2PA cross section (σ_2). To this end, we have to consider the role of the local electrostatics in two-photon absorptivity and, particularly, in its vibronic intensity distribution.

The $S_0 \rightarrow S_1$ electronic transition is simultaneously allowed for one- and two-photon absorption processes in the red FP chromophore; see Figure 1. This is not surprising because the chromophore structure has very low symmetry and its $S_0 \rightarrow S_1$ transition has appreciable CT character.[9] While the integrated 1PA strength is proportional to the corresponding transition dipole moment matrix element ($\boldsymbol{\mu}$) squared, its 2PA counterpart contains an additional factor equal to the square of the difference between the permanent dipole moments in the excited ($\boldsymbol{\mu}_1$) and ground ($\boldsymbol{\mu}_0$) states, $\Delta\boldsymbol{\mu} = \boldsymbol{\mu}_1 - \boldsymbol{\mu}_0$. This latter factor is present because of the considering of both the ground (S_0) and the excited (S_1) states as intermediate states in the sum-over-states expression of the 2PA tensor.[25,26] Therefore, one of the key molecular parameters driving strong variations of the 2PA properties of the red FP chromophore is $\Delta\boldsymbol{\mu}$, which in turn is sensitive to variations of local electric field.[27] If a strong electric field $\mathbf{E}$ is applied along the chromophore main axis, the permanent dipole moments in both the ground and excited states will change and $\Delta\boldsymbol{\mu}$ will acquire an additional induced part, which will add up to the inherent vacuum part, $\Delta\boldsymbol{\mu}_{vac}$, yielding the linear dependence of total $\Delta\boldsymbol{\mu}$ on $\mathbf{E}$: $\Delta\boldsymbol{\mu} = \Delta\boldsymbol{\mu}_{vac} + {}^1/_2\Delta\alpha\mathbf{E}$, where $\Delta\alpha$

Received: November 15, 2011
Revised: December 21, 2011
Published: January 6, 2012

   dx.doi.org/10.1021/jp211020k | J. Phys. Chem. B 2012, 116, 1736−1744

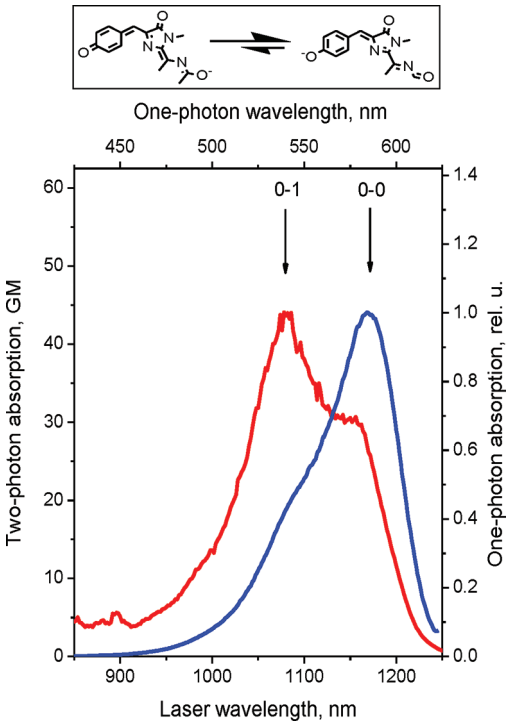

Figure 1. One-photon (blue line, right *y*-axis) and two-photon (red line, left *y*-axis) absorption spectra of mRFP.[9] For easier comparison, the top *x*-axis shows the one-photon absorption wavelength and the bottom *x*-axis shows the laser wavelength, used for two-photon excitation. The inset shows two limiting resonance structures of the red FP chromophore. The arrows depict the pure electronic (0−0) transition dominating in one-photon absorption and the vibronic (0−1) transition intensified in the two-photon absorption spectrum. Note that at room temperature the position of the 1PA spectral maximum usually almost coincides with the 0−0 transition due to a presence of the hot-band absorption from thermally populated soft vibrational modes.

is the difference between the polarizabilities of the excited and ground states.

A special feature of the red FP chromophore is that there is a specific vibrational coordinate that is intrinsically coupled to $\Delta\boldsymbol{\mu}$. Shown in Figure 1 are the two limiting resonating forms pertinent to the anionic red FP chromophore,[28] where the actual chromophore structure at a certain value of **E** adopts an intermediate configuration between the two. In the simple model, initially suggested by Marder, Brédas, Perry, and co-authors[29,30] for the description of nonlinear optical properties of dipolar chromophores with CT resonance, the gradual transition from one limiting structure to another results in a concerted stretching/contracting of adjacent double/single bond lengths with the concomitant CT in the ground state, eventually connected with the change of $\Delta\boldsymbol{\mu}$;[29−32] see Scheme 1 in the Supporting Information. Therefore, we can expect that this particular, bond-length-alternating (BLA), vibrational coordinate will be inherently coupled to $\Delta\boldsymbol{\mu}$.

In the past, several theoretical models have been proposed to explain the vibronic intensity gain in the 2PA spectrum. Most have focused on symmetric (namely, centrosymmetric or quasi-centrosymmetric) molecules, where the electronically forbidden by symmetry 2PA transition becomes allowed due to the Herzberg−Teller (HT) coupling of an electronic transition dipole moment ($\boldsymbol{\mu}$) to a vibration with an appropriate symmetry.[33−37] In this situation, in the expansion of transition dipole moment into the Taylor series over the vibrational coordinate, the second term, containing the first derivative of $\boldsymbol{\mu}$ over the coordinate becomes the dominant one, resultung in the shift of the whole vibronic progression to higher frequencies by a vibrational quantum. However, the FP chromophore has very low symmetry, so these models do not apply.

Recently, vibronic effects in 2PA spectra of noncentrosymmetrical and dipolar (push−pull) molecules with $\Delta\boldsymbol{\mu} \neq 0$ have been considered theoretically. Painelli et al. considered vibrationally excited states (in the electronic ground and excited manifolds) as intermediate states in the sum-over-states expression.[32] These authors have shown that the HT coupling of transition dipole moment ($\boldsymbol{\mu}$), but not $\Delta\boldsymbol{\mu}$, to a certain vibration can result in a domination of the corresponding vibronic peak in the 2PA spectrum of a push−pull molecule. The authors of refs 38−42 applied the Herzberg−Teller approximation to describe the intensity distribution in the two-photon transitions of the lowest-energy $S_0 \rightarrow S_1$ electronic band. In the case of aniline[38] and model anionic GFP chromophore, 4-hydroxybenzylidene-2,3-dimethylimidazoline,[42] certain vibronic transitions were predicted to strongly dominate over the pure electronic one in the 2PA spectrum. However, the role of the vibronic coupling of $\Delta\boldsymbol{\mu}$ to the BLA coordinate has not been explicitly demonstrated in these works.

Here, we propose a physical model that quantitatively explains the effect of the enhancement of the vibronic 2PA transition in a dipolar FP chromophore by explicitly considering the effect of the Herzberg−Teller-type coupling of the permanent dipole moments difference $\Delta\boldsymbol{\mu}$ to the BLA vibrational coordinate. We also consider the important interference effect between the "Herzberg−Teller" amplitude of this kind and the Franck−Condon amplitude associated with the coupling of transition dipole moment $\boldsymbol{\mu}$ to the same vibrational mode, and show that this effect is crucial in explaining the great 2PA intensity of some FPs, such as DsRed and tdTomato.

2. RESULTS AND DISCUSSION

2.1. Survey of Experimental Data. *2.1.1. Linear Absorption and Fluorescence Properties. Rule of "Mirror Symmetry".* In the red FPs studied here, the first electronic $S_0 \rightarrow S_1$ 1PA transition is strongly dipole-allowed and shows a descending vibronic progression with domination of the pure electronic (0−0) peak; see Figure 1. The 1PA peak wavelengths (λ_{1PA}), extinction coefficients (ε_m), and the change of the permanent dipole moment ($|\Delta\boldsymbol{\mu}|$) upon $S_0 \rightarrow S_1$ excitation (corresponding to the 0−0 transition) have been characterized previously and are presented in Table 1.

Vibronic intensity distribution in one-photon absorption and fluorescence spectra of organic molecules is usually described with the so-called basic model,[43] which is based on (1) Franck−Condon approximation (transition dipole moment does not depend on vibrational coordinates); (2) harmonic approximation for potentials in the electronic ground and excited states; (3) assumption that upon electronic excitation the nuclear system experiences only the shift(s) of equilibrium positions but not the change of frequencies or system of normal coordinates. To validate this model experimentally, one can check if the absorption and fluorescence spectra are "mirror-symmetrical" to each other with respect to the vertical line passing through their intersection point. Figure 2 presents the normalized excitation and fluorescence spectra of the red FPs. For quantitative inspection of the "mirror symmetry" rule, we also present the fluorescence spectrum, symmetrically reflected

dx.doi.org/10.1021/jp211020k | J. Phys. Chem. B 2012, 116, 1736−1744

Table 1. One-Photon Absorption, Two-Photon Absorption, and Fluorescence Properties of FPs[a]

protein	λ_{1PA}, nm	ε_m, $M^{-1}cm^{-1}$	$\lvert\Delta\boldsymbol{\mu}_e\rvert$, D	β	λ_{2PA}, nm	$\bar{\nu}_a$, cm^{-1}	$\varepsilon(\lambda_{2PA}/2)/\varepsilon_m$	σ_{2max}, GM
mTangerine	567	35000	1.0 ± 0.1	0.075	1055	1320	0.50	15
mStrawberry	576	60000	1.4 ± 0.2	0.126	1070	1290	0.57	20
mCherry	589	74000	2.2 ± 0.2	0.071	1080	1510	0.41	27
mPlum	590	65000	2.6 ± 0.2	0.086	1105	1200	0.50	29
mRFP	586	73000	2.8 ± 0.3	0.105	1080	1420	0.40	44
mCherry (at pH 11)	565	72000	3.5 ± 0.4	0.151	1080	790	0.63	70
DsRed2	562	86000	3.6 ± 0.4	0.215	1050	1120	0.42	100
tdTomato	557	80000	3.7 ± 0.4	0.203	1050	1160	0.50	140

[a]Experimental data on the one-photon absorption maximum wavelength λ_{1PA}, maximum extinction coefficient ε_m, change of permanent dipole moment upon excitation $\lvert\Delta\boldsymbol{\mu}_e\rvert$, two-photon absorption maximum wavelength λ_{2PA}, and maximum two-photon absorption cross section σ_{2max} are obtained from the literature.[9,27] The parameter of the mirror symmetry β, frequency of vibronic transition, responsible for 2PA maximum $\bar{\nu}_a$, and the relative 1PA intensity at the wavelength corresponding to the 2PA maximum $\varepsilon(\lambda_{2PA}/2)/\varepsilon_m$ are calculated in this work; see text.

with respect to the line defined above. Further, we define a parameter of "mirror symmetry", β, as a root-mean-square of the deviation of normalized excitation spectrum from the mirror-inversed normalized fluorescence spectrum, i.e.,

$$\beta = \left(\frac{\int (A(\nu) - F(\nu))^2 \, d\nu}{\int (A(\nu))^2 \, d\nu} \right)^{1/2}$$

where $A(\nu)$ and $F(\nu)$ are the excitation and mirror-inversed fluorescence spectra, respectively. The calculated β values are presented in Table 1. By definition, β tends to zero if the spectra are perfectly mirror symmetric.

If β is smaller than the Born–Oppenheimer parameter $\chi = (m_e/M)^{1/4} \approx 0.1$, where m_e is the electron mass and M is a typical nuclear reduced mass, then the basic model holds.[43] As one can see, the latter condition is satisfied for most of the proteins, with the exception of mCherry (at pH 11), DsRed2, and tdTomato, where $\beta > 0.15$. There are two possibilities for the violation of the basic model: either the Franck–Condon approximation fails, or the system of normal coordinates/vibrational frequencies changes upon excitation.[43] The first case is pertinent to the dipole-forbidden transitions, and does not apply here. It follows therefore that, in mCherry (at pH 11), DsRed2, and tdTomato, there is some vibrational coordinate, whose force constant changes considerably upon electronic excitation. The most probable vibration of this kind is that which changes the adjacent bond lengths (i.e., from single to double and vice versa), i.e., involves bond length alternations.[43] In the following, we will see how the coupling of this vibrational mode to electronic transition dipole moment can lead to a strong interference between Franck–Condon and "Herzberg–Teller" components of the two-photon absorption in these three proteins.

2.1.2. One-Photon versus Two-Photon Absorption Spectra: Vibronic Intensity Redistribution. Figure 3 and Figure S1 in the Supporting Information compare the previously published[9,27] 2PA spectra with 1PA spectra of red FPs in the region of their $S_0 \rightarrow S_1$ electronic transition. The 2PA spectra were obtained[9,27] by plotting the integrated fluorescence signal versus excitation wavelength with all necessary corrections to variations of laser parameters and with quantitative calibration of the spectrum to the known 2PA cross section of a reference dye. In the 1PA spectrum, the lowest-frequency pure electronic transition dominates, but the 2PA peak is shifted to the blue by a vibrational frequency $\bar{\nu}_a$. The $\bar{\nu}_a$ values for all the FPs (estimated as a difference between the 2PA and 1PA peak frequencies) are listed in Table 1. The 0–0 transition is also present in the 2PA spectrum (as a shoulder on the low-frequency side), but it is always weaker than the vibronic one. Note that, for the mCherry (at pH 11), DsRed2, and tdTomato, where the mirror symmetry rule was distorted, the values of vibrational frequencies are systematically lower than those for the other proteins. Table 1 also presents the relative 1PA intensity at the wavelength corresponding to the 2PA maximum ($\varepsilon(\lambda_{2PA}/2)/\varepsilon_m$).

2.2. Physical Model of Vibronic Transitions in the 2PA Spectrum. Our model of vibronic transitions in the $S_0 \rightarrow S_1$ manifold is based on the following assumptions.

(1) Adiabatic approximation for both 1PA and 2PA transitions (which is sometimes called Born–Oppenheimer approximation) considers the total molecular wave function as a product of electronic $\psi_f(r,Q)$ and vibrational $\varphi_{fn}(Q)$ parts:

$$\Psi_{fn}(r, Q) = \psi_f(r, Q)\varphi_{fn}(Q) \quad (1)$$

where f is an electronic quantum number, n is a vibrational quantum number, r are the electronic coordinates, and Q is the manifold of normal vibrational coordinates.

(2) Harmonic approximation of the potential energy for the nuclear motion in electronic ground and excited states.

(3) The 1PA spectrum is described within the Franck–Condon approximation (for all vibrational modes) which means that the electronic transition dipole moment $\boldsymbol{\mu}_e$ between the ground, 0, and excited, 1, states, where index e refers to the pure electronic matrix element, does not depend on nuclear coordinates. This approximation usually holds for dipole-allowed transitions. In this case, the matrix element of the total (vibronic) transition dipole moment is

$$\begin{aligned} \boldsymbol{\mu} &= \langle 0|\boldsymbol{\mu}_e(Q)|n\rangle \\ &= \langle 0|\boldsymbol{\mu}_e(Q^0)|n\rangle \\ &= \boldsymbol{\mu}_e(Q^0)\langle 0|n\rangle \end{aligned} \quad (2)$$

where Q^0 is a set of fixed equilibrium values of Q

$$\boldsymbol{\mu}_e(Q^0) = \boldsymbol{\mu}_e = \langle \psi_1(r, Q^0)|\boldsymbol{\mu}|\psi_0(r, Q^0)\rangle \quad (3)$$

and vibrational wave functions are

$$|0\rangle \equiv \varphi_{0,0}, \qquad |n\rangle \equiv \varphi_{1,n} \quad (4)$$

Here and in the following, we consider for simplicity only transitions originating from the lowest vibrational level

dx.doi.org/10.1021/jp211020k | J. Phys. Chem. B 2012, 116, 1736–1744

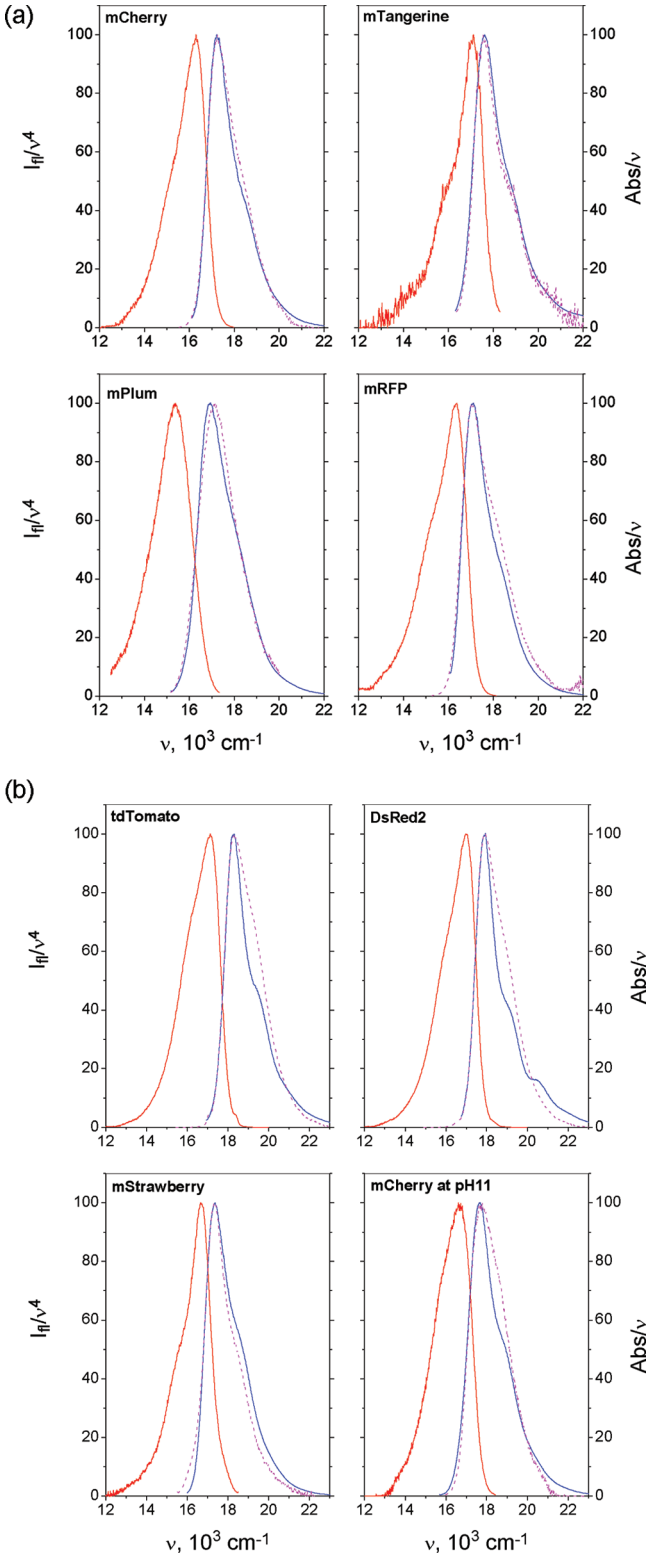

Figure 2. Excitation (continuous blue line), fluorescence (continuous red line),[9,27] and mirror-reflected fluorescence (dashed magenta line) spectra of red FPs. All spectra are corrected and presented in quanta per frequency interval.

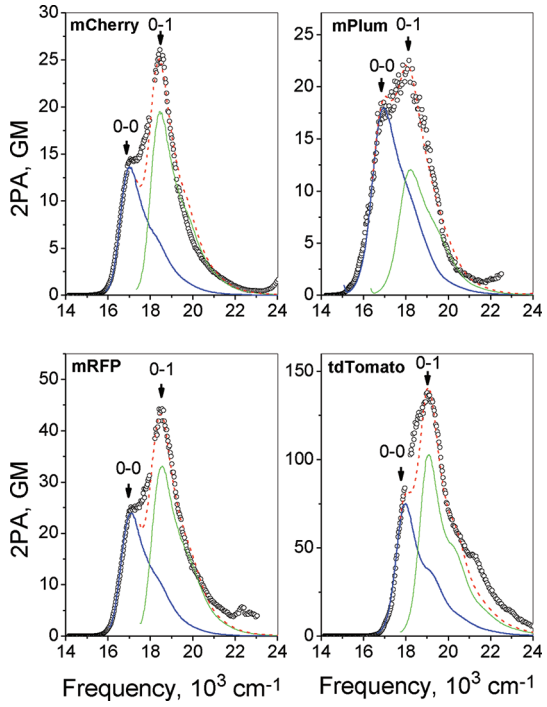

Figure 3. Two-photon (open circles) and one-photon (blue continuous line) absorption spectra of red FPs[9] presented versus transition frequency, which is equal to twice the laser frequency in the case of two-photon excitation. The 2PA spectral shape is fitted to the sum of two 1PA spectral shapes (red dashed line), one corresponding to the actual 1PA spectrum with variable amplitude (blue continuous line) and another to a 1PA spectrum shifted to a higher frequency, where the shift and the amplitude were varied (green continuous line).

of the ground electronic state (corresponding to stiff vibrations with frequencies $\nu > kT/h$). Note that, within these approximations, the 1PA vibronic spectrum is completely determined by the dependence of Franck–Condon factors $|\langle 0|n\rangle|^2$ on n and on the shift of equilibrium positions in S_1 versus S_0 (i.e., Huang–Rhys factors).

(4) We use the two-level approximation[44−48] for the 2PA vibronic transitions (0–0, 0–1, etc.). This approximation is justified by the following: (a) Quantum mechanical calculations show that 95% of the total 2PA cross section of the $S_0 \rightarrow S_1$ transition in the GFP-type chromophore is described exclusively by the two-level model (dipolar term) (P. R. Callis, personal communication). (b) The 1PA transitions to the higher electronic levels ($S_0 \rightarrow S_n$), which could contribute to the 2PA tensor, are strongly forbidden.[3,9,49] (c) Two-level approximation is consistent with the quantitative description of the quadratic Stark effect in the proteins under consideration.[27]

(5) The two-photon absorption tensor **S** is one-dimensional, with the transition dipole moment $\boldsymbol{\mu}$ and change of permanent dipole moment $\Delta\boldsymbol{\mu}$ aligned along the same axis. This is usually true for the chromophores with a quasi-one-dimensional π-conjugation system of electrons. An independent support for this assumption stems from the Stark spectroscopy results, showing that the angle between $\boldsymbol{\mu}$ and $\Delta\boldsymbol{\mu}$ in DsRed is quite small, ~13°.[50]

With approximations 4 and 5, the electronic part of the 2PA tensor can be written, up to a known constant factor, as[25,26]

$$S_e = \Delta\mu_e\mu_e \qquad (5)$$

dx.doi.org/10.1021/jp211020k | J. Phys. Chem. B 2012, 116, 1736–1744

where $\Delta\mu_e = |\Delta\boldsymbol{\mu}|$ and $\mu_e = |\Delta\boldsymbol{\mu}_e|$.

The two-photon vibronic amplitudes are described by the matrix elements of the two-photon tensor between appropriate vibrational wave functions:[39]

$$S_{0,n} = \langle 0|S_e(Q)|n\rangle \tag{6}$$

If we then apply the Franck–Condon method, assuming that the electronic part of the 2PA tensor does not depend on nuclear coordinates ($S_e(Q) = S_e(Q^0)$) in eq 6, we would obtain exactly the same vibronic progression as in the case of 1PA (no redistribution of intensity), which is, however, inconsistent with experimental observations. Further, the transition dipole moment μ is a common factor in both 1PA and 2PA vibronic amplitudes and, thus, its potentially possible dependence on Q would not explain the difference between 1PA and 2PA spectra. This leads us to the next key assumptions:

(6) The $\Delta\mu_e$ value depends on a certain normal vibrational coordinate Q_a, $\Delta\mu_e = \Delta\mu_e(Q_a)$. Physically, the stretching of a double bond and alternative contraction of an adjacent conjugated single bond, i.e., BLA vibration, should be intimately coupled to the charge shift (i.e., $\Delta\mu_e$) upon excitation; see Scheme 1 in the Supporting Information. We assume that this vibration contributes significantly to a normal mode Q_a.

(7) We suppose that $\Delta\mu_e$ depends on Q_a linearly at least in the region of the changes of Q_a. We therefore present this dependence as a series expansion up to the linear term:

$$\Delta\mu_e = \Delta\mu_e(Q_a^0) + \left[\frac{\partial\Delta\mu_e}{\partial Q_a}\right]_{Q_a^0} Q_a \tag{7}$$

where Q_a^0 is the equilibrium position of coordinate Q_a. The first term corresponds to a pure electronic contribution, and the second term can be called the "Herzberg–Teller" term in analogy with that occurring in Taylor expansion of μ_e. However, there is an important difference between the Herzberg–Teller approximation used for description of transition dipole moments in symmetrical molecules and that considered here for the change of the permanent dipole moment. In symmetrical molecules, the term $[\partial\mu_e/\partial Q]_{Q^0}Q$ is a small correction to the main, $\mu_e(Q^0)$, term if the 1PA transition is dipole-allowed. Alternatively, it becomes dominant for symmetry-forbidden transitions, when $\mu_e(Q^0) = 0$.[43] Contrary to these two limiting situations, in the case of dipolar CT molecules, $\Delta\mu_e(Q_a^0)$ can vary continuously in response to varying electric field, from 0 to some maximum value μ_{max}, while $[\partial\Delta\mu_e/\partial Q_a]_{Q_a^0}$ remains essentially constant, i.e., $[\partial\Delta\mu_e/\partial Q_a]_{Q_a^0} = (\partial\Delta\mu_e/\partial Q_a) = \text{const}$ (see discussion of Scheme 1 in the Supporting Information). Therefore, the 0–0 and 0–1 2PA transitions originating from the first and second terms of eq 7, respectively, can have comparable intensities (see eqs 8–14 below), which would be unlikely for symmetrical molecules.

The neglect of higher-order terms in eq 7 will be justified for the series of FPs under study in what follows (see Figure 4 and discussion thereafter). Substituting eq 7 into eq 5 and then the result into eq 6, we get for the vibronic matrix element of S:

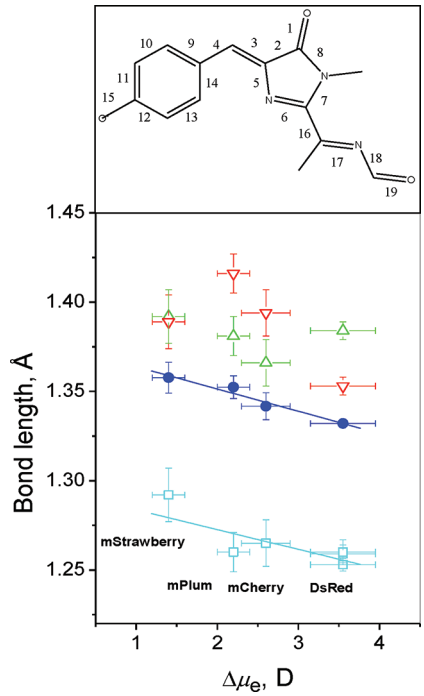

Figure 4. Dependence of chemical bond lengths in the chromophore on the change of permanent dipole moment upon excitation. Data points with different $\Delta\mu_e$ values correspond to various FP mutants. The chemical structure of the chromophore is shown in the top inset. The open squares correspond to bond number 15, open up triangles to bond number 4, and open down triangles to bond number 5. The closed circles correspond to the arithmetic mean of the three.

$$S_{0,n} = \langle 0|S_e|n\rangle = \Delta\mu_e(Q_a^0)\mu_e\langle 0|n\rangle + \frac{\partial\Delta\mu_e}{\partial Q_a}\mu_e\langle 0|Q_a|n\rangle \tag{8}$$

Summing over all excited vibrational states of the S_1 manifold in eq 8, substituting the actual constant factor associated with the 2PA tensor in eq 5, taking the modulus square, averaging over all isotropic orientations of molecular dipoles, and taking into account the local field correction in dielectric, we obtain the dependence of the 2PA cross section on frequency (2PA spectrum):

$$\sigma_2 = A\left[\Delta\mu_e^2(Q_a^0)\mu_e^2\sum_n g(\nu - \nu_{00} - \sum_k \nu_k n_k)\right.$$
$$W_n + \mu_e^2\left(\frac{\partial(\Delta\mu_e)}{\partial Q_a}\right)^2$$
$$\left.\sum_{n,m} g(\nu - \nu_{00} - \sum_k \nu_k n_k - \nu_a m)HT_m W_n\right] \tag{9}$$

where $W_n = \prod_k e^{-s_k}(s_k^{n_k}/n_k!)$, s_k is the Huang–Rhys factor, $n_k = 0, 1, 2, \ldots$ is the vibrational quantum number, and ν_k is the eigenfrequency for the kth normal mode, $m = 0, 1, 2, \ldots$ is the vibrational quantum number of the ath mode, ν_{00} is the optical frequency of the pure electronic transition, $g(\Delta\nu)$ is the

dx.doi.org/10.1021/jp211020k | J. Phys. Chem. B 2012, 116, 1736–1744

normalized lineshape function ($\int_{-\infty}^{\infty} g(\Delta\nu)\,d\Delta\nu = 1$) of an individual vibronic transition, where the detuning $\Delta\nu = \nu - \nu_{max}$ is the difference between the doubled laser frequency $\nu = 2\nu_l$ and the particular vibronic transition peak ν_{max}. The constant factor A reads[46]

$$A = \frac{32}{5}\frac{(\pi L)^4}{(hcn)^2} \tag{10}$$

where h is the Planck constant, c is the speed of light, n is the refractive index, and $L = (n^2 + 2)/3$ is the Lorentz local field factor. The Herzberg–Teller factor entering eq 9 can be easily calculated (e.g., ref 39)

$$HT_m = |\langle 0|Q_a|m\rangle|^2 = \frac{\hbar}{4\pi M_a \nu_a} e^{-s_a} \frac{s_a^{(m-1)}}{m!}(s_a - m)^2 \tag{11}$$

Note that in eq 9 we do not consider a possible effect of interference between the amplitudes of the first, FC, and second, "HT", terms. It will be shown later that in some proteins this interference cannot be neglected.

Equation 9 can be further simplified if one assumes a very small shift of equilibrium position along Q_a upon electronic excitation ($s_a \approx 0$). This assumption is justified by Figure S2 in the Supporting Information, and here, we notice that in this case only the transition with $m = 1$ is nonvanishing, cf. eq 11, and equal to

$$HT_1 \approx \frac{\hbar}{4\pi M_a \nu_a} \tag{12}$$

Applying this to eq 9, we obtain

$$\sigma_2 = A\left[\Delta\mu_e^2(Q_a^0)\mu_e^2 \sum_n g(\nu - \nu_{00} - \sum_k \nu_k n_k) W_n + \left(\frac{\partial(\Delta\mu_e)}{\partial Q_a}\right)^2 \frac{\hbar}{4\pi M_a \nu_a}\mu_e^2 \sum_n g(\nu - \nu_{00} - \sum_k \nu_k n_k - \nu_a) W_n\right] \tag{13}$$

In the above equation, the combination $\mu_e^2 \sum_n g(\nu - \nu_{00} - \sum_k \nu_k n_k) W_n$ is nothing but the appropriately normalized one-photon absorption spectrum (with the condition $\int_0^{\infty} \sum_n g(\nu - \nu_{00} - \sum_k \nu_k n_k) W_n\,d\nu = 1$), which we can designate as $K(\nu)$ and thus arrive to the final expression for σ_2:

$$\sigma_2 = A\left[\Delta\mu_e^2(Q_a^0)K(\nu) + \left(\frac{\partial(\Delta\mu_e)}{\partial Q_a}\right)^2 \frac{\hbar}{4\pi M_a \nu_a} K(\nu - \nu_a)\right] \tag{14}$$

By inspecting the structure of eq 14, one can see that the 2PA spectrum is described by a sum of two components: the first having exactly the same shape as the 1PA spectrum and the amplitude proportional to $\Delta\mu_e^2(Q_a^0)$ which originates from the Franck–Condon part of the $\Delta\mu_e$ expansion and the second also having the same shape as the 1PA spectrum but shifted to higher frequencies by ν_a and with the amplitude proportional to $(\partial(\Delta\mu_e)/\partial Q_a)^2(\hbar/4\pi M_a \nu_a)$, which originates from the "Herzberg–Teller" term.

2.2. Comparison of Experimental Data with the Model. *2.2.1. Simulation of Experimental 2PA Spectra with the Model eq 14.* Figure 3 shows the 2PA spectra of mCherry, mPlum, mRFP, and tdTomato (see Figure S1 in the Supporting Information for the rest of the series) with the attempts to fit them to a sum of two 1PA spectral profiles: one not shifted but with the variable amplitude (FC-contribution) and the other shifted to the blue by vibronic frequency ν_a (which was a variable parameter) and with variable amplitude ("HT"-contribution). The total 1PA profile was not varied and was taken from the experiment. Figure 3 and Figure S1 (Supporting Information) show that the spectra of mCherry, mPlum, and mRFP can be fitted quite well, although those of other FPs are poorly fit. Therefore, we can conclude that the 2PA spectra of at least mCherry, mPlum, and mRFP can be qualitatively described by the above model withouot taking into account the interference between FC and "HT" terms. A possible relation of this behavior of mCherry, mPlum, and mRFP to some similarities in their structure is discussed later in the text.

2.2.2. Identification of Vibrational Mode Coupled to $\Delta\mu_e$ and Estimation of the Coupling Strength. The goal of this part of the work is to search for correlations between the change of permanent dipole moment $\Delta\mu_e$ and the chromophore structure in order to identify which particular bonds contribute to the BLA vibrational mode and estimate the corresponding coupling strength. Table S1 in the Supporting Information summarizes the bond lengths in the conjugated structure of the chromophore for several FPs whose high resolution crystallographic data are available[51−53] and also presents the bond lengths encountered in *p*-benzoquinone and hydrated sodium phenoxide for comparison. The effective BLA parameter is not easy to evaluate for the integral π-conjugated system of the chromophore because of its strongly heterogeneous structure (compared, e.g., to polyenes).[54] Therefore, we first investigated possible correlations between the $\Delta\mu_e$ values and particular bond lengths in the chromophore. Note that since the Q_a and Q_a^0 represent the same physical coordinate, the dependence of $\Delta\mu_e$ on Q_a^0 can be used to obtain the $\partial(\Delta\mu_e)/\partial Q_a$ value. The best correlation, shown in Figure 4 with open squares, has been found for the phenoxide C—O bond (bond number 15, Figure 4 inset). As one can see, this bond length (l_{15}) varies within the limits determined by the maximum possible value, corresponding to the single C—O$^-$ bond in hydrated sodium phenoxide (1.331 Å) and the minimum possible value, corresponding to the double C═O bond in *p*-benzoquinone (1.222 Å), which suggests that the real C—O bond in the red FP chromophore always has an intermediate order between 1 and 2. With $\Delta\mu_e$ increasing, this bond systematically shortens from $l_{15} = 1.292$ (in mStrawberry) to 1.253 Å (in DsRed). The fact that the dependence is linear justifies assumption 7 of the model. The slope of the linear regression to the data points provides $|\partial Q_a/\partial(\Delta\mu_e)| = 0.013 \pm 0.004$ Å/D and therefore the coupling parameter $(\partial(\Delta\mu_e)/\partial Q_a)^2 = (6 \pm 4) \times 10^3$ D^2/Å^2. It is interesting that, although other bond lengths show individually worse correlation than l_{15}, the sum of l_{15}, l_4, and l_5 correlates with $\Delta\mu_e$ even better ($R = -0.976$, SD = 0.0030, $P = 0.024$) than l_{15} alone

dx.doi.org/10.1021/jp211020k | J. Phys. Chem. B 2012, 116, 1736−1744

(R = −0.835, SD = 0.0085, P = 0.038). This finding is quite reasonable because all three bonds are expected to change their lengths in phase (either stretch or contract) in response to changes of $\Delta\mu_e$. Figure 4 also shows the dependence of the l_4, l_5, and the average $\langle l\rangle = {}^1/_3\,(l_{15} + l_4 + l_5)$ on $\Delta\mu_e$. Due to statistical averaging of the standard deviations, we were able to obtain smaller error margins for the coupling parameter in this case: $(\partial(\Delta\mu_e)/\partial Q_a)^2 = (6.4 \pm 1.9) \times 10^3$ D^2/Å^2.

2.2.3. Quantitative Description of the Peak 2PA Cross Section. To describe quantitatively the dependence of the peak 2PA cross section on $\Delta\mu_e$, we first make use of the relation:[55]

$$K(\nu) = \frac{3 \times 10^3 \ln 10 hc}{(2\pi)^3 N_A} \frac{n}{L^2} \frac{\varepsilon(\nu)}{\nu} \tag{15}$$

where ε is the extinction coefficient (in M^{-1} cm^{-1}) and N_A is the Avogadro number. Substituting eq 15 and eq 10 into eq 14 and noticing that $K(\nu_{00} + \nu_a)/K(\nu_{00}) = \varepsilon(\lambda_{2PA}/2)/\varepsilon_m$, we obtain for the peak 2PA vibronic transition strength

$$\sigma_{2,\max} = \frac{12\pi 10^3 \ln 10}{5hcN_A} \frac{L^2}{n} \frac{\varepsilon_m}{\nu_{01}} \left(\Delta\mu_e^2 (Q_a^0) \frac{\varepsilon(\lambda_{2PA}/2)}{\varepsilon_m} + \left(\frac{\partial(\Delta\mu_e)}{\partial Q_a} \right)^2 \frac{\hbar}{4\pi M_a \nu_a} \right) \tag{16}$$

Substituting for n = 1.33 (for water), $\bar{\nu}_{01}$ = 18600 cm^{-1} (average optical transition frequency of the 2PA peak), and $\varepsilon(\lambda_{2PA}/2)/\varepsilon_m$ the values from Table 1 and expressing σ_2 in GM (1 GM = 10^{-50} cm^4 s) and $\Delta\mu_e$ in D (1 D = 10^{-18} esu), we obtain

$$\sigma_{2,\max} = 3.23 \times 10^{-5} \varepsilon_m \left(\Delta\mu_e^2 (Q_a^0) \frac{\varepsilon(\lambda_{2PA}/2)}{\varepsilon_m} + \left(\frac{\partial(\Delta\mu_e)}{\partial Q_a} \right)^2 \frac{\hbar}{4\pi M_a \nu_a} \right) \tag{17}$$

Figure 5 shows the dependence of both one-photon (ε_m) and two-photon ($\sigma_{2,\max}$) molecular absorptivities on $\Delta\mu_e$. The slow linear increase of ε_m can be explained by a weak perturbation of electronic wave functions in the ground and excited states, and, consequently, of the transition dipole moment μ_e by the electric field **E**.[56] The best linear fit to the experimental data is

$$\varepsilon_m(\Delta\mu_e) = 24 \times 10^3 + 16 \times 10^3 \Delta\mu_e \tag{18}$$

It is clear from Figure 5 that the 2PA peak increases nonlinearly, especially for $\Delta\mu_e$ > 3 D. Our attempts to fit the whole σ_2 data set to function 17, even with eq 18 taken into account, failed because the experimentally observed dependence was much steeper than the third order polynomial, provided by eqs 17 and 18 combined. Recalling that, in mCherry (pH 11), DsRed2, and tdTomato the "mirror symmetry" of absorption and fluorescence spectra was violated, and so the "HT"/FC interference possibly shows up in the 2PA spectrum, we decided to apply eqs 17 and 18 to the first five experimental points only, i.e., to those with $\Delta\mu_e$ < 3 D, and then return to the description of mCherry (pH11), DsRed2, and tdTomato. We then have fixed parameter $\varepsilon(\lambda_{2PA}/2)/\varepsilon_m$ equal to 0.5, i.e., an average value for the five proteins under consideration (Table 1). The resulting fit of experimental data to the function $y = 3.23 \times 10^{-2}(24 + 16x)(0.5x^2 + C)$ (originating from eqs 17 and 18) with the single fitting parameter C is shown in Figure 5 by a solid black line. It describes the experimental data reasonably well and yields C = 13 ± 1 D^2. By inspection of eq 17, we see that $C = (\partial(\Delta\mu_e)/\partial Q_a)^2(\hbar/4\pi M_a \nu_a)$. The only undefined parameter left in this expression is the reduced mass M_a. Taking advantage of the known values of $\bar{\nu}_a$ = 1350 cm^{-1} (average for the first five proteins in Table 1) and $(\partial(\Delta\mu_e)/\partial Q_a)^2 = (6.4 \pm 1.9) \times 10^3$ D^2/Å^2 (found previously), we estimate $M_a \approx 11 \times 10^{-24}$ g ≈ (6 ± 2) m_p, where m_p is the proton mass. This number agrees rather well with the reduced mass of an isolated C−O, C−C, or C−N stretching vibration (M = 6−7 m_p), as well as with the reduced masses found for collective modes in benzene and its simple derivatives (M = 6 − 12 m_p),[57] thus strongly supporting our model.

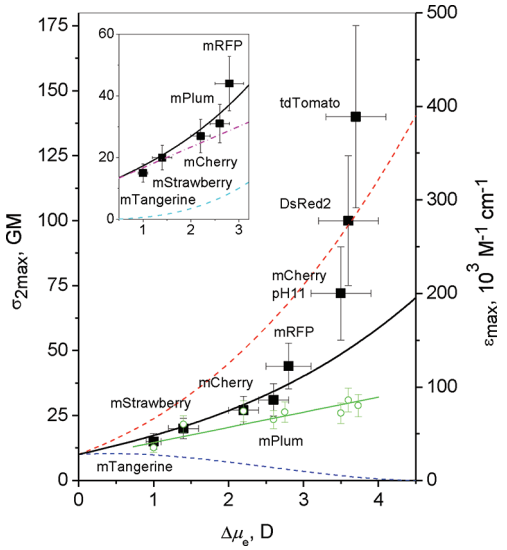

Figure 5. Dependence of one-photon absorption maximum extinction (green open circles) and two-photon absorption maximum cross section (black closed squares) on the change of permanent dipole moment upon excitation. One-photon data are fitted with a linear function (continuous green line). The first five points of the 2PA data are fitted to model eq 17 (continuous black line); see text. The inset shows the first five experimental points with the Franck−Condon (blue dashed line) and "Herzberg−Teller" (magenta dashed−dotted line) contributions to eq 17, as well as their sum (black continuous line). The red dashed line of the main plot represents the case of constructive interference between FC and "HT" terms, and the blue dashed line, the case of destructive interference.

The inset in Figure 5 shows the magnified version of the same plot with the fitting function 17 as well as the separate contributions due to the Franck−Condon (FC) part (σ_2^{FC} = $3.23 \times 10^{-2}(24 + 16\Delta\mu_e) \times 0.5\Delta\mu_e^2$) and the "Herzberg−Teller" ("HT") part ($\sigma_2^{HT} = 3.23 \times 10^{-2}(24 + 16\Delta\mu_e) \times 13$). As one can see, the "HT" term dominates the 2PA response in all cases; however, the FC contribution becomes appreciable for mCherry, mPlum, and, particularly, mRFP.

2.2.4. Interference between FC and "HT" Terms. The lack of "mirror symmetry" between absorption and fluorescence spectra of mCherry (pH 11), DsRed2, and tdTomato strongly suggests that a contribution from a vibrational coordinate that has considerably different force constants in the ground and excited states can emerge in the 1PA spectrum as a vibronic transition originating from the FC coupling of this coordinate to μ_e.

dx.doi.org/10.1021/jp211020k | J. Phys. Chem. B 2012, 116, 1736−1744

As discussed before, this vibration, containing a significant contribution from the same (BLA) coordinate, also strongly couples to $\Delta\mu_e$, resulting in the "HT" vibronic peak of the 2PA spectrum. Since the same vibration can be present in the total FC distribution originating from the μ_e part of the 2PA tensor (first term in eq 17), it can interfere with the "HT" term, represented by the second term of eq 17. A possible reason for why the FC/"HT" interference starts to play a crucial role for these three proteins is that their vibrational frequency ν_a is lower, compared to that of the other proteins (cf. $\bar{\nu}_a$ = 800−1100 cm^{-1} for mCherry (pH 11), DsRed2, and tdTomato vs 1200−1500 cm^{-1} for the rest of the series). The decreased frequency probably comes to better resonance with the most prominent frequency, FC-coupled to μ_e (Fermi resonance). The interference between FC and HT terms in the 1PA spectrum both due to a coupling of the same vibration to μ_e was previously described in the literature,[58,59] but here we deal with the interference between two 2PA transitions, one FC-coupled to μ_e and another "HT"-coupled to $\Delta\mu_e$. To take this effect into account quantitatively, we modify eq 17 as follows:

$$\sigma_{2,\max} = 3.23 \times 10^{-5}\varepsilon_m(\Delta\mu_e)(\mathrm{FC} + \mathrm{HT} \pm 2\sqrt{\mathrm{FC} \times \mathrm{HT}}) \quad (19)$$

where we introduce the notations $\mathrm{FC} = \Delta\mu_e^2\varepsilon(\lambda_{2PA}/2)/\varepsilon_m$ and $\mathrm{HT} = (\partial(\Delta\mu_e)/\partial Q_a)^2(\hbar/4\pi M_a\nu_a)$. The plus sign corresponds to constructive interference, and the minus sign, to destructive. Making use of the parameters found previously (for the situation without interference), we present function 19 in Figure 5 for both cases of constructive and destructive interference. As one can see, the behavior of mCherry (pH 11), DsRed2, and tdTomato can be reasonably well described in terms of constructive interference between FC and "HT" terms.

3. CONCLUSIONS

The 2PA properties of many FP mutants have been recently characterized,[9] but their relation to the chromophore and protein structure was not completely understood. The new physical model presented here explains the intensification of the vibronic transition in the 2PA spectra of a series of red FPs through the "Herzberg−Teller" coupling of the permanent dipole moment change $\Delta\mu_e$ to the BLA vibrational coordinate. It also describes quantitatively the variation of the corresponding transition strength in a series of mutants with the same red FP chromophore by considering a combined action of the Franck−Condon and "Herzberg−Teller" parts of vibronic interaction with possible interference between them. The model is potentially applicable to a wide class of ionic and zwitterionic fluorophores possessing resonating structures.

■ ASSOCIATED CONTENT

Supporting Information

Scheme 1 shows the "two-form, two-state" model, relating the change of permanent dipole moment upon excitation with the weight of resonating form B in the red FP chromophore. Figure S1 presents the decomposition of the two-photon absorption spectrum on to the sum of two 1PA spectral profiles, one corresponding to the actual 1PA spectrum with variable amplitude (Franck−Condon part) and another to the 1PA spectrum shifted to a higher frequency, where the shift and the amplitude were varied ("Herzberg−Teller" part). Figure S3 shows the calculated vibronic spectra due to only Herzberg−Teller coupling with the varying values of the Huang−Rhys factor. Table S1 contains the available literature data on the lengths of chemical bonds in red FP chromophore in a series of red FPs and in some relative molecules. This material is available free of charge via the Internet at http://pubs.acs.org.

■ ACKNOWLEDGMENTS

This work was supported by the National Institute of General Medical Sciences grant R01 GM086198. We thank P. R. Callis for useful discussions.

■ REFERENCES

(1) Blab, G. A.; Lommerse, P. H. M.; Cognet, L.; Harms, G. S.; Schmidt, T. *Chem. Phys. Lett.* **2001**, *350*, 71−77.
(2) Spiess, E.; Bestvater, F.; Heckel-Pompey, A.; Toth, K.; Hacker, M.; Stobrawa, G.; Feurer, T.; Wotzlaw, C.; Berchner-Pfannschmidt, U.; Porwol, T.; et al. *J. Microsc.* **2005**, *217*, 200−204.
(3) Drobizhev, M.; Makarov, N. S.; Hughes, T.; Rebane, A. *J. Phys. Chem. B* **2007**, *111*, 14051−14054.
(4) Ivanchenko, S.; Glaschick, S.; Röcker, C.; Oswald, F.; Wiedenmann, J. *Biophys. J.* **2007**, *92*, 4451−4457.
(5) Hosoi, H.; Yamaguchi, S.; Mizuno, H.; Miyawaki, A.; Tahara, T. *J. Phys. Chem. B* **2008**, *112*, 2761−2763.
(6) Drobizhev, M.; Tillo, S.; Makarov, N. S.; Hughes, T. E.; Rebane, A. *J. Phys. Chem. B* **2009**, *113*, 855−859.
(7) Hashimoto, H.; Isobe, K.; Suda, A.; Kannari, F.; Kawano, H.; Mizuno, H.; Miyawaki, A.; Midorikawa, K. *Appl. Opt.* **2010**, *49*, 3323−3329.
(8) Tillo, S.; Hughes, T. E.; Makarov, N. S.; Rebane, A.; Drobizhev, M. *BMC Biotechnol.* **2010**, *10* (6).
(9) Drobizhev, M.; Makarov, N. S.; Tillo, S. E.; Hughes, T. E.; Rebane, A. *Nat. Methods* **2011**, *8*, 393−399.
(10) Clark, T. B.; Orr, M. E.; Flynn, D. C.; Goodson, T. III. *J. Phys. Chem. C* **2011**, *115*, 7331−7338.
(11) Aslanidi, E. B.; Tikhonov, E. A. *Opt. Spectrosc.* **1974**, *37*, 446−447.
(12) Xu, C.; Webb, W. W. *J. Opt. Soc. Am. B* **1996**, *13*, 481−491.
(13) Wakebe, T.; van Keuren, E. *Jpn. J. Appl. Phys.* **1999**, *38*, 3556−3561.
(14) Scherer, D.; Dörfler, R.; Feldner, A.; Vogtmann, T.; Schwoerer, M.; Lawrentz, U.; Grahn, W.; Lambert, C. *Chem. Phys.* **2002**, *279*, 179−207.
(15) Cogné-Laage, E.; Allemand, J.-F.; Ruel, O.; Baudin, J.-B.; Croquette, V.; Blanchard-Desce, M.; Jullien, L. *Chem.—Eur. J.* **2004**, *10*, 1445−1455.
(16) Fu, J.; Padilha, L. A.; Hagan, D. J.; Van Stryland, E. W.; Przhonska, O. V.; Bondar, M. V.; Slominsky, Y. L.; Kachkovski, A. D. *J. Opt. Soc. Am. B* **2007**, *24*, 56−66.
(17) Makarov, N. S.; Drobizhev, M.; Rebane, A. *Opt. Express* **2008**, *16*, 4029−4047.
(18) Padilha, L. A.; Webster, S.; Przhonska, O. V.; Hu, H.; Peceli, D.; Rosch, J. L.; Bondar, M. V.; Gerasimov, A. O.; Kovtun, Y. P.; Shandura, M. P.; et al. *J. Mater. Chem.* **2009**, *19*, 7503−7513.
(19) Hales, J. M.; Matichak, J.; Barlow, S.; Ohira, S.; Yesudas, K.; Brédas, J.-L.; Perry, J. W.; Marder, S. R. *Science* **2010**, *327*, 1485−1488.
(20) Beuerman, E.; Makarov, N. S.; Drobizhev, M.; Rebane., A. *Proc. SPIE* **2010**, *7599*, 75990X.
(21) Butko, M. T.; Drobizhev, M.; Makarov, N. S.; Rebane, A.; Brinkman, B. C.; Gleeson, J. G. *BMC Biotechnol.* **2011**, *11* (20).
(22) Yanushevich, Y. G.; Staroverov, D. B.; Savitsky, A. P.; Fradkov, A. F.; Gurskaya, N. G.; Bulina, M. E.; Lukyanov, K. A.; Lukyanov, S. A. *FEBS Lett.* **2002**, *511*, 11−14.
(23) Campbell, R. E.; Tour, O.; Palmer, A. E.; Steinbach, P. A.; Baird, G. S.; Zacharias, D. A.; Tsien, R. Y. *Proc. Natl. Acad. Sci. U.S.A.* **2002**, *99*, 7877−7882.
(24) Shaner, N. C.; Campbell, R. E.; Steinbach, P. A; Giepmans, B. N. G.; Palmer, A. E.; Tsien, R. Y. *Nat. Biotechnol.* **2004**, *22*, 1567−1572.

(25) Callis, P. R.; Scott, T. W.; Albrecht, A. C. *J. Chem. Phys.* **1981**, *75*, 5640−5646.
(26) Dick, B.; Hohlneicher, G. *J. Chem. Phys.* **1982**, *76*, 5755−5760.
(27) Drobizhev, M.; Tillo, S.; Makarov, N. S.; Hughes, T. E.; Rebane, A. *J. Phys. Chem. B* **2009**, *113*, 12860−12864.
(28) Gross, L. A.; Baird, G. S.; Hoffman, R. C.; Baldridge, K. K.; Tsien, R. Y. *Proc. Natl. Acad. Sci. U.S.A.* **2000**, *97*, 11990−11995.
(29) Meyers, F.; Marder, S. R.; Pierce, B. M.; Brédas, J. L. *J. Am. Chem. Soc.* **1994**, *116*, 10703−10714.
(30) Lu, D.; Chen, G.; Perry, J. W.; Goddard, W. A. III. *J. Am. Chem. Soc.* **1994**, *116*, 10679−10685.
(31) Barzoukas, M.; Runser, C.; Fort, A.; Blanchard-Desce, M. *Chem. Phys. Lett.* **1996**, *257*, 531−537.
(32) Painelli, A.; Del Freo, L.; Terenziani, F. *Chem. Phys. Lett.* **2001**, *346*, 470−478.
(33) Aleksandrov, A. P.; Bredikhin, V. I.; Genkin, V. N. *Sov. Phys.−JETP* **1971**, *33*, 1078−1082.
(34) Goodman, L.; Rava, R. P. *Adv. Chem. Phys.* **1983**, *54*, 177−230 andreferences therein.
(35) Callis, P. R. *Annu. Rev. Phys. Chem.* **1997**, *48*, 271−297 and references therein.
(36) Ohira, S.; Rudra, I.; Schmidt, K.; Barlow, S.; Chung, S.-J.; Zhang, Q.; Matichak, J.; Marder, S. R.; Brédas, J.-L. *Chem.—Eur. J.* **2008**, *14*, 11082−11091.
(37) Terenziani, F.; Przhonska, O. V.; Webster, S.; Padilha, L. A.; Slominsky, Y. L.; Davydenko, I. G.; Gerasov, A. O.; Kovtun, Y. P.; Shandura, M. P.; Kachkovski, A. D.; et al. *J. Phys. Chem. Lett.* **2010**, *1*, 1800−1804.
(38) Callis, P. R. *Chem. Phys. Lett.* **1984**, *107*, 125−130.
(39) Macak, P.; Luo, Y.; Ågren, H. *Chem. Phys. Lett.* **2000**, *330*, 447−456.
(40) Macak, P.; Luo, Y.; Norman, P.; Ågren, H. *J. Chem. Phys.* **2000**, *113*, 7055−7061.
(41) Lin, N.; Zhao, X.; Rizzo, A.; Luo, Y. *J. Chem. Phys.* **2007**, *126*, 244509.
(42) Kamarchik, E.; Krylov, A. I. *J. Phys. Chem. Lett.* **2011**, *2*, 488−492.
(43) Frank-Kamenetskii, M. D.; Lukashin, A. V. *Sov. Phys.−Uspekhi.* **1975**, *18*, 391−409.
(44) Birge, R. R.; Zhang, C.-F. *J. Chem. Phys.* **1990**, *92*, 7178−7195.
(45) Delysse, S.; Raimond, P.; Nunzi, J.-M. *Chem. Phys.* **1997**, *219*, 341−351.
(46) Drobizhev, M.; Meng, F.; Rebane, A.; Stepanenko, Y.; Nickel, E.; Spangler, C. W. *J. Phys. Chem. B* **2006**, *110*, 9802−9814.
(47) Rebane, A.; Makarov, N. S.; Drobizhev, M.; Spangler, B.; Tarter, E. S.; Reeves, B. D.; Spangler, C. W.; Meng, F.; Suo, Z. *J. Phys. Chem. B* **2008**, *112*, 7997−8004.
(48) Rebane, A.; Drobizhev, M.; Makarov, N. S.; Beuerman, E.; Haley, J. E.; Krein, D. M.; Burke, A. R.; Flikkema, J. L.; Cooper, T. M. *J. Phys. Chem. A* **2011**, *115*, 4255−4262.
(49) Olsen, S.; McKenzie, R. H. *Chem. Phys. Lett.* **2010**, *492*, 150−156.
(50) Lounis, B.; Deich, J.; Rosell, F. I.; Boxer, S. G.; Moerner, W. E. *J. Phys. Chem. B* **2001**, *105*, 5048−5054.
(51) Wang, L.; Jackson, W. C.; Steinbach, P. A.; Tsien, R. Y. *Proc. Natl. Acad. Sci. U.S.A.* **2004**, *101*, 16745−16749.
(52) Shu, X.; Shaner, N. C.; Yarbrough, C. A.; Tsien, R. Y.; Remington, S. J. *Biochemistry* **2006**, *45*, 9639−9647.
(53) Shu, X.; Wang, L.; Colip, L.; Kallio, K.; Remington, S. J. *Protein Sci.* **2009**, *18*, 460−466.
(54) Laino, T.; Nifosi, R.; Tozzini, V. *Chem. Phys.* **2004**, *298*, 17−28.
(55) Toptygin, D. *J. Fluoresc.* **2003**, *13*, 201−219.
(56) Bublitz, G. U.; Boxer, S. G. *Annu. Rev. Phys. Chem.* **1997**, *48*, 213−242.
(57) Belau, L.; Haas, Y. *Chem. Phys. Lett.* **2001**, *333*, 297−303.
(58) Osadko, I. S. *Opt. Spectrosc.* **1972**, *32*, 259−263.
(59) Hohlneicher, G.; Wolf, J. *Bunsen-Ges. Phys. Chem., Ber.* **1995**, *99*, 366−370.